The Aeronautical Journal (2025), **129**, pp. 3665–3686
doi:10.1017/aer.2025.10063

ROYAL AERONAUTICAL SOCIETY

RESEARCH ARTICLE

Performance reliability and parameter sensitivity analysis of spacecraft separation system combining Monte Carlo and Adaboost regression methods

S. Lai[1,2], T. Wang[3], Q. Zhao[1,3], C. Wang[1] and J. Chen[1]

[1]Nanjing University of Aeronautics and Astronautics, Nanjing 211106, China
[2]National Key Laboratory of Aerospace Mechanism, Shanghai 201109, China
[3]Shanghai Institute of Aerospace Systems Engineering, Shanghai 201109, China
Corresponding author: Chen Wang; Email: nuaawangchen@nuaa.edu.cn

Received: 11 September 2024; **Revised:** 24 July 2025; **Accepted:** 24 July 2025

Keywords: Adaboost; aerospace mechanism; Monte Carlo; separation dynamics; spacecraft

Abstract

The Monte Carlo methods are frequently employed to evaluate the overall characteristics of non-monotonic, non-linear, non-superpositional performance functions. However, the multi-parameter, multi-objective spacecraft separation dynamics model is not amenable to decoupling to produce a result. This paper presents a parametric objective function that can be sampled. It combines the reliability analysis of the complex non-linear spacecraft separation model with Automated Dynamic Analysis of Mechanical Systems (ADAMS) and uses the Monte Carlo method to obtain the separation performance of the spacecraft separation system reliability profile, that is to say, the distribution of separation performance. The performance distribution of the spacecraft separation system was determined and parameters such as spring separation force, spring line of action, module mass and module centre of mass position were found to have a significant effect on the spacecraft separation dynamics by Adaboost machine learning regression.

Nomenclature

U	upper compartment
L	lower compartment
rel	relative
V	separation velocity
a	acceleration
α	angular acceleration
J	moment of inertia
ω	angular velocity
$\mathbf{M}$	torque
F	force
s	displacement
r_i	actual value of the deviation parameter
μ_i	mean deviation
σ_i	standard deviation
f	maximum force deviation of springs
ΔF_i	working force deviation relative to reference spring
θ_i	force line angle deviation
$f_{i,final}$	spring residual force deviation

© The Author(s), 2025. Published by Cambridge University Press on behalf of Royal Aeronautical Society.

https://doi.org/10.1017/aer.2025.10063 Published online by Cambridge University Press

Abbreviations

Adaboost	adaptive boosting
ADAMS	Automated Dynamic Analysis of Mechanical Systems
ADRC	active disturbance rejection control
RSM	response surface method
SIASE	Shanghai Institute of Aerospace Systems Engineering

1.0 Introduction

All types of space shuttles in service still need to be delivered by a carrier into a predetermined orbit after launch [1]. Once on orbit, the separation between the shuttle and the carrier is critical to help save fuel and other resources and increase the efficiency and success of the mission, but this process is uncertain and uncontrollable [2]. There are variables in the performance of the separation device, and once the motion attitude of the separated upper and lower modules is beyond the regulation range of the control system, the whole separation mission will face a great safety risk [3]. Shown in Fig. 1, the combination of reusable spacecraft complish the seperation mission on orbit. The separation system contains seven sets of active and passive separation thrust resistance, including four sets of separation springs that generate separation thrust, two sets of separation breakers that generate separation thrust before providing separation resistance and one set of separation plugs that provide separation resistance throughout.

It is therefore evident that the study of the dynamics of the spacecraft separation system and the investigation of the reliability and impact of the energy storage device within the separation system [4] have been pivotal areas of research within the field of aerospace engineering. Hu X et al. used a multi-island genetic algorithm to optimise the design of separation springs with the objective of separation accuracy [5]. B. N. Rao et al. systematically described the application of rigid body dynamics in inter stag. The mechanical characteristics of the separation process were dynamically simulated and analysed, providing a basis for the optimised design of the separation system [6]. Saman Saki et al. developed an optimised adaptive soft-switching multi-model predictive control strategy for spacecraft attitude control under a wide range of operating conditions, improving the robustness and control accuracy of the system [7]. Wei-Jie Li et al. reviewed the development of on-orbit servicing technologies and discussed key challenges and recent progress in their technical implementation, in particular the application of separation and docking technologies [8]. Ding et al. studied the shock mitigation technology during the spacecraft-rocket separation process through numerical simulation and experiment, and the results show that the optimally designed separation mechanism can effectively reduce the shock load and ensure the safety of the separation process [9]. Fu et al. proposed a quasi-smooth mode control strategy based on neural network for spacecraft attitude manoeuvre control, which ensures the robustness of the system under the specified performance index [10]. Hou et al. designed and experimentally verified a disturbance force application unit to simulate spacecraft separation, and the test results verified the effectiveness and accuracy of the unit in simulating the separation process [11]. Lyu et al. investigated a T-S fuzzy attitude control strategy based on intermediate observers, and proposed a hybrid non-fragile control method for the input saturation problem, which improved the attitude control performance of the flexible spacecraft [12]. Hu et al. explored the application of active disturbance rejection control (ADRC) in multi-body spacecraft separation, and ensured the safety and stability of the separation process through a composite control strategy [13].

At present, the research methods employed to determine the optimal design of the separation system are inadequate, as they fail to provide a comprehensive study of the separation process as a whole. The existing theoretical models lack sufficient complexity, and the environmental conditions under which the system operates are not sufficiently considered. Furthermore, the study of the key parameters of the separation system is inadequate. Luo et al. investigated the autonomous separation dynamics of a spaceborne multi-rigid body system with uncertain parameters, providing theoretical analysis and practical guidance for complex separation systems [14]. Teng et al. put forth a composite optimisation method for the position of the separation spring, integrating angular velocity and external moment [15].

https://doi.org/10.1017/aer.2025.10063 Published online by Cambridge University Press

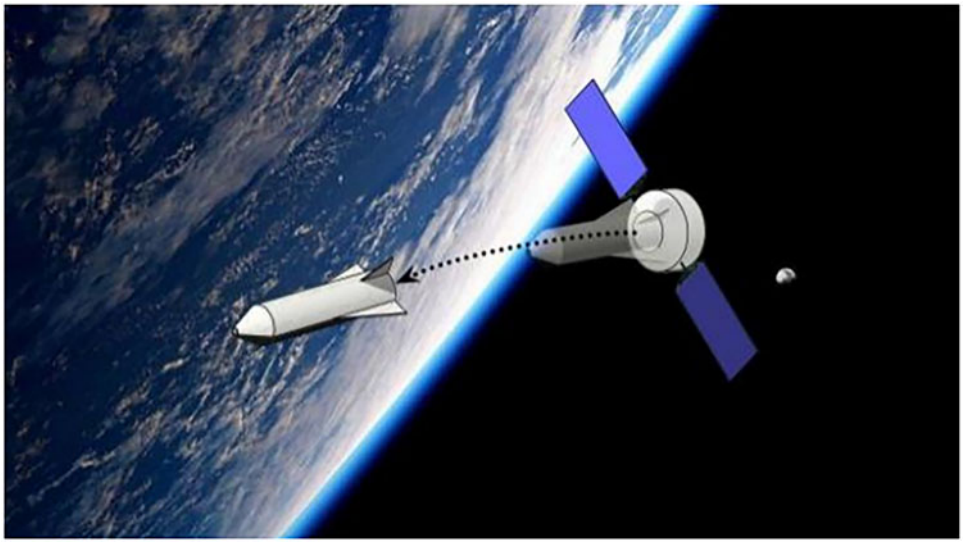


Figure 1. *Separation mission of reusable spacecraft on orbit.*

In order to verify the reliability of the separation performance, parameter sensitivity analyses are carried out with the post-separation spacecraft attitude parameters as the evaluation target.

For example, Cui D et al. used the nonlinear response surface method (RSM) to point out the structural parameters in the rigid envelope [3] that are significantly sensitive to the spacecraft separation dynamics, but the response surface method itself is a class of agent modelling methods, which approximates the implicit limit state function through polynomials, and is unable to solve the decoupling analysis of the whole spacecraft separation dynamics in the presence of high-dimensional variable parameters effectively. However, the separation process takes place in a highly complex mechanical environment, and in addition to errors in the release efficiency of the energy storage system, errors such as the mass properties and mechanical characteristics of the separation module are also important factors affecting the separation attitude [2].

The advantage of the Monte Carlo method lies in its suitability for solving problems involving multiple continuous random variables (high dimensions). The Monte Carlo method, based on the gambler's theory, is a statistical simulation algorithm that randomly samples input parameters to form a sample set, providing approximate solutions through a large number of simulations. Theoretically, the larger the sample size, the closer the results are to the true value.

Adaptive boosting (Adaboost) is an iterative algorithm that employs a training set to train and aggregate multiple weak classifiers into a stronger final classifier. The Adaboost algorithm itself is implemented by varying the distribution of the data, which is based on the correctness of the classification of each sample in the training set and the overall classification of the last sample in the training set. The overall classification accuracy of the last sample determines the weights for each sample. The updated dataset with revised weights is then transmitted to the lower classifier for training purposes. The resulting classifiers are subsequently integrated to form the final decision classifier. The majority of research on the Adaboost algorithm, as well as its applications, is currently focused on classification problems. However, there have also been some emerging applications in regression problems in recent years. In terms of its applications, the Adaboost series is primarily employed in the resolution of two-class problems, multi-class single-label problems, multi-class multi-label problems, large class single-label problems, and regression problems. It learns with the full training sample. The Adaboost classifier enables the exclusion of superfluous features from the training data, thereby focusing attention on the most pertinent elements [16–18].

https://doi.org/10.1017/aer.2025.10063 Published online by Cambridge University Press

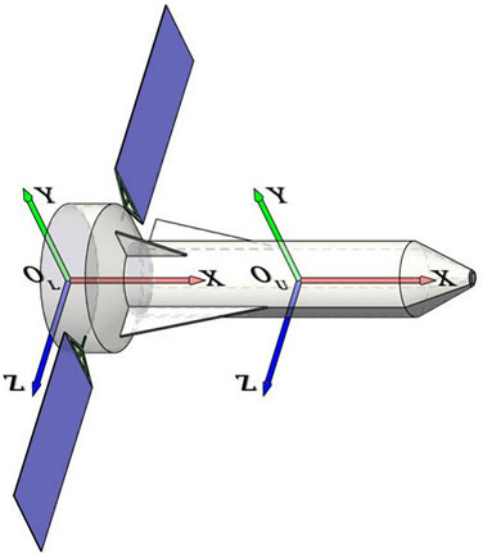


Figure 2. *Coordinate systems of separation motion.*

2.0 Problem formulation

The evaluation indexes of the separation motion of the upper and lower modules mainly include the relative separation speed, module separation overload, module angular velocity and relative distance. In order to express the above indexes, it is necessary to define the co-ordinate system related to each rigid body of the separation system, in which is the centroid co-ordinate system of modules, and the base co-ordinate system is the centroid co-ordinate system of the lower module. The spacecraft attitude is described by the relationship between the three axes of the spacecraft body co-ordinate system and the three axes of the orbit co-ordinate system, both of them are right-handed orthogonal co-ordinate systems, and co-ordinate systems are given in Fig. 2. X-axis direction as the positive direction of separation.

In Fig. 3, red circles represent seven sets of forces, from 1 to 4 are separation springs, 5 and 6 are separation disconnectors, and the separation plug is 7. Because of the deviation between separation springs and the asymmetrical layout of forces, the dissociative motion state of modules might be disturbed. In fact, the mission will be decided failure if the separate velocity can not reach the stated objective that was set for entering orbit, or collision happened between upper and lower module.

In deriving the kinetic equations, the upper and lower compartment modules are considered as homogeneous rigid bodies. The nonlinear model of separation system of reusable spacecraft contains input and output relationship of multiple parameters. According to the dynamics of the spatial motion multi-rigid body system, where the descriptive equations for the main parameters are as follows Newton-Euler equations [19]:

1) Relative separation speed between modules

$$V_{rel} = V_U - V_L \tag{1}$$

V_U, V_L are the centre-of-mass velocities of the upper and lower module, the upper module velocity V_U for example:

$$V_U = \int_0^t a_U dt \tag{2}$$

https://doi.org/10.1017/aer.2025.10063 Published online by Cambridge University Press

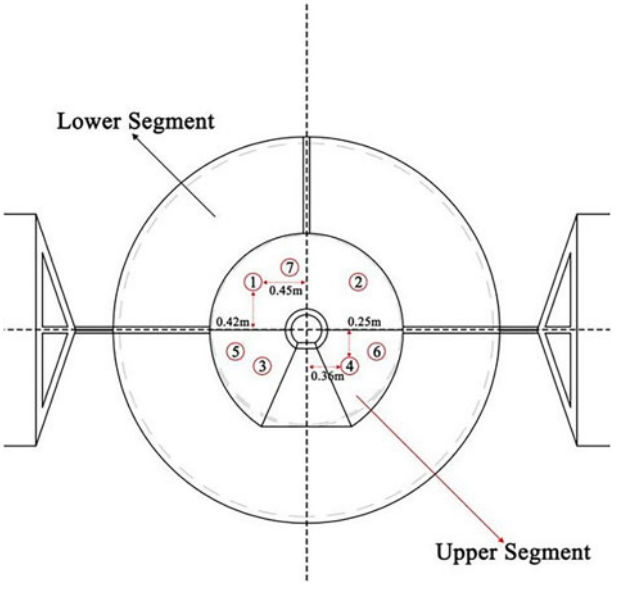


Figure 3. *Forces distributed on contact surface of modules.*

a_U is the centre-of-mass acceleration of the upper module:

$$a_U = \dot{V}_U = \frac{F_U}{m_U} \tag{3}$$

$$F_U = \sum_{i=1}^{7} f_i \tag{4}$$

2) Angular acceleration of separation of the upper module

$$J_U \cdot \dot{\omega}_U + \omega_U \times (J_U \cdot \omega_U) = \mathbf{M}_U \tag{5}$$

$$\alpha_U = \dot{\omega}_U = \frac{\mathbf{M}_U - \omega_U \times (J_U \cdot \omega_U)}{J_U} \tag{6}$$

$$\mathbf{M}_U = \sum_{i=1}^{7} \mathbf{M}_{U,i} \tag{7}$$

$$\mathbf{M}_{U,i} = r_{U,i} \times f_i \tag{8}$$

$$r_{U,i} = D_{U,i} - C_U \tag{9}$$

$$\omega_U = \int_0^t \alpha_U dt \tag{10}$$

3) Overload of separation of lower module

$$a_L = \dot{V}_L = \frac{F_L}{m_L} \tag{11}$$

$$g_L = \frac{a_L}{G} \tag{12}$$

https://doi.org/10.1017/aer.2025.10063 Published online by Cambridge University Press

4) Relative distance between upper and lower module

$$\Delta s = s_U - s_L \tag{13}$$

$$s_U = \int_0^t V_U dt \tag{14}$$

$$s_L = \int_0^t V_L dt \tag{15}$$

Using the dynamics simulation technology of Automated Dynamic Analysis of Mechanical Systems (ADAMS) software, we import the simplified combined model of the separated system into it and directly solve the attitude parameters after separation. We mainly focus on the overall separated attitude of the upper and lower modules, and perform Boolean operations on the upper and lower modules separately after importing into ADAMS to reduce the number of parts in the overall model. In ADAMS, in addition to the local coordinate system of the part, there is a global coordinate system that coincides with the above coordinate system.

3.0 Dynamic simulation of spacecraft separation event

The upper and lower modules are separated by a series of components, including springs, a separation plug and disconnectors. The seven sets of external forces, as well as the contact surfaces that may generate contact between the upper and lower modules, were set up using the ADAMS built-in dynamics model and the mathematical and displacement function statements in the runtime function.

The separating direction of the upper module is positive, i.e. in the direction of the X-axis, and the force between the upper and lower modules mainly consists of the spring force generated by the four sets of springs, which is a positive separating thrust for the upper module and a reaction force of opposite magnitude and direction for the lower module.

There are two sets of disconnectors between the upper and lower modules. The disconnectors provide a thrust to the upper module at the beginning of the separation section, 0–0.01 m, and a resistance to the upper module at the end of the separation section, 0.01–0.0442 m, and the forces acting on the lower module are equal in magnitude and opposite in direction.

In addition to the above seven sets of external forces, there is a separating plug between the upper and lower modules, which produces a separating resistance on the upper module when the relative displacement distance between the upper and lower modules reaches 0.01, with a value of 80 N, which rapidly decreases to 0 after the displacement increment reaches 0.002 m.

It is the work of this section to transform the force under the above conditions into a time-varying function and to introduce the numerical model of the separation system for calculation. In addition, it should be noted that the disconnectors and seperation plugs do not have a deviation from the line of force.

According to Figs. 4 and 5, it can be analysed that the initial force of the separation spring acting on the upper module is 2102 N, i.e., the preload is 2102 N. The force decreases linearly from 0 to 0.1073 s, and the value is 533.5 N at 0.1073 s. The spring force no longer decreases after that, and it can be concluded that its time of action is 0.1073 s, and it is 0.1073 s for the ideal working condition.

It can be seen that the separation spring separation thrust has a large influence on the separation attitude of the upper and lower modules, and the asymmetric spring layout has a cross-strong external moment on its Y-axis, which generates a certain angular acceleration and angular velocity, and then generates angular displacement. And the angular velocity, relative velocity, and separation overload between the upper and lower modules can be used as the evaluation indexes of the separation performance to analyse the reliability and parameter sensitivity of the spacecraft separation dynamics performance.

https://doi.org/10.1017/aer.2025.10063 Published online by Cambridge University Press

https://doi.org/10.1017/aer.2025.10063 Published online by Cambridge University Press

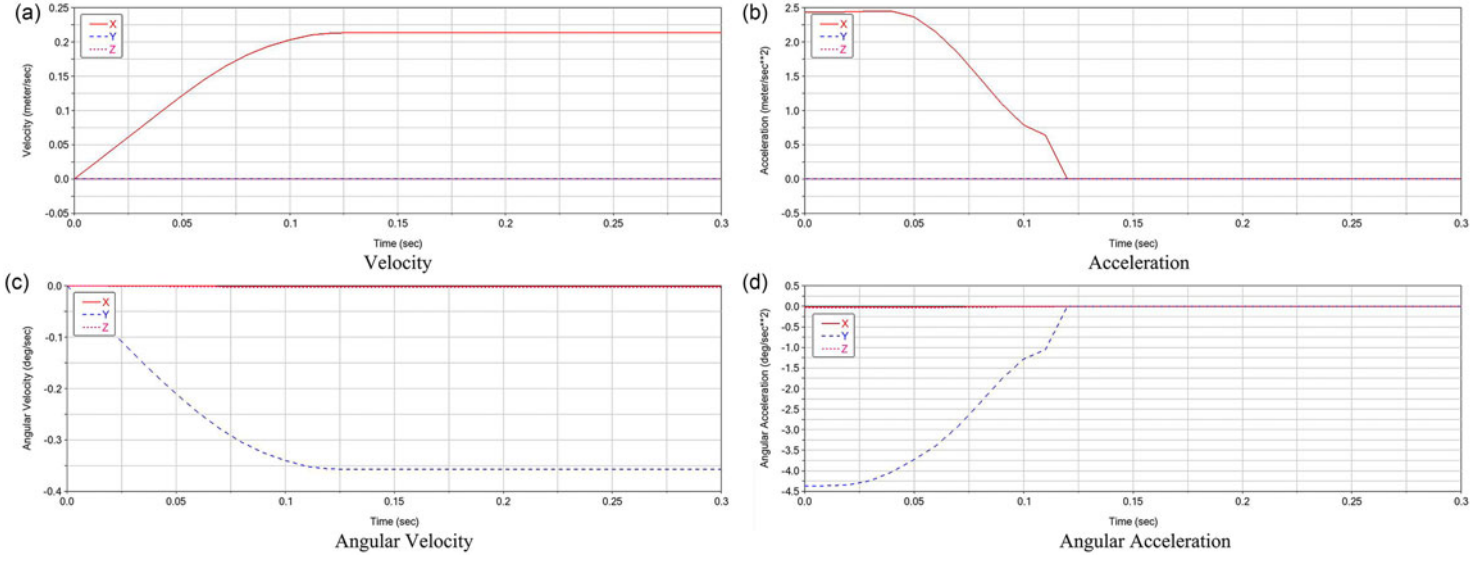


Figure 4. *Upper module separation attitude.*

https://doi.org/10.1017/aer.2025.10063 Published online by Cambridge University Press

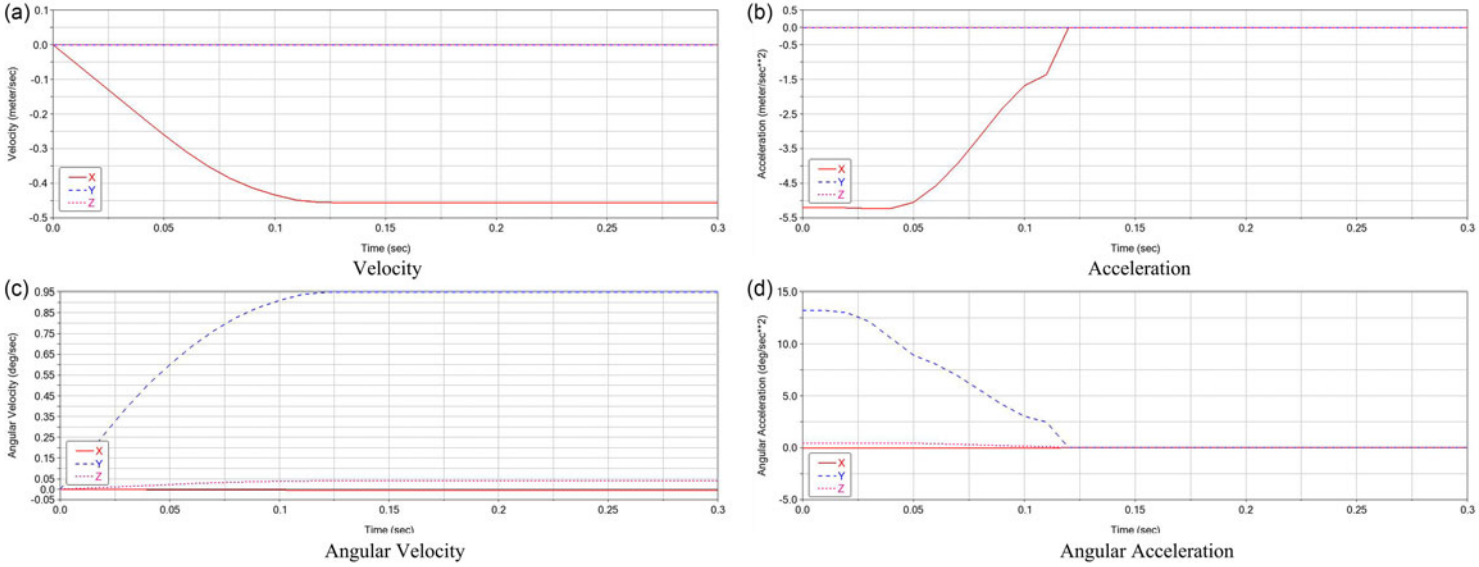


Figure 5. *Lower module separation attitude.*

Table 1. *Internal deviations of the separation system*

Deviations	Range
$f_{i,initial}$(N)	2177±75
ΔF_i(N)	±25
θ_i(°)	±0.6883
$f_{i,final}$(N)	533.5±30

*The variable distribution probabilities all follow a normal distribution

Table 2. *Deviation of quality characteristics*

Deviations	Upper		Lower	
Mass(kg)	3016.9±15		1417.2±40	
X(m)	5.336±0.016		0.725±0.026	
Y(m)	−0.001±0.01		−0.002±0.01	
Z(m)	0.037±0.011		−0.043±0.011	
J_{XX}(kg · m^2)	1150		1930	
J_{YY}(kg · m^2)	13041	±10%	1041	±10%
J_{ZZ}(kg · m^2)	13403		1872	

*The variable distribution probabilities all follow a normal distribution

4.0 Numerical analysis simulation results

After the verification of model accuracy and reasonableness, this section brings a new method to assess the reliability and sensitivity analysis of spacecraft whole star separation performance based on Monte Carlo method.

Model with deviation parameter

$$f(r_i)_{(r_{i\min}\le x\le r_{i\max})}=\int_{r_{i\min}}^{r_{i\max}}\frac{1}{\sqrt{2\pi}\cdot\sigma_i}e^{-\frac{(r_i-\mu_i)^2}{2(\sigma_i)^2}}dr_i \tag{16}$$

Where r_i is the actual value of the deviation parameter, μ_i and σ_i are the mean and standard deviation, respectively, assuming that the upper and lower limits of the inputs are $r_{i\min}$ and $r_{i\max}$, respectively. then its mean value can be derived, which is:

$$\mu_i=\frac{1}{2}(r_{i\min}+r_{i\max}) \tag{17}$$

According to the principle of 3σ, the standard deviation can be found to be:

$$\sigma_i=\frac{1}{6}(r_{i\min}-r_{i\max}) \tag{18}$$

The deviation parameters are specified in Tables 1 and 2, starting with the internal deviations of the separation system.

Measurement objects are established for the performance indicators that are to be observed and collected, and they can be observed during the simulation process, with the specific names corresponding to those shown in the Table 3.

Establish the simulation target that needs to collect data, the name of the simulation target, and the type of data to be collected during the simulation as shown in the Table 4.

The last step in setting up the simulation test is to create a simulation script. Due to the large number of model components, simulation model variables and simulation objectives, the calculation process is complex, so after several rounds of comparison, the optimal script termination time and step size were finally determined, where the termination time is 0.2 s and the step size is 0.01 s.

https://doi.org/10.1017/aer.2025.10063 Published online by Cambridge University Press

Table 3. *Measurement objects*

Measurement Name
Angular_Velocity_U_Amp
Angular_Velocity_U_x
Angular_Velocity_U_y
Angular_Velocity_U_z
CONTACT_F_MEA
Relative_Velocity_Amp
Relative_Velocity_x
Relative_Velocity_y
Relative_Velocity_z
Separation_Overload_of_L_Amp
Separation_Overload_of_L_x
Separation_Overload_of_L_y
Separation_Overload_of_L_z
Delta_Displacement_M_53_54

Table 4. *Simulation target*

Simulation Target Name	Note
OBJ_Angular_Velocity_U_Amp	maximum
OBJ_Angular_Velocity_U_x	minimum
OBJ_Angular_Velocity_U_y	minimum
OBJ_Angular_Velocity_U_z	minimum
OBJ_CONTACT_F_MEA	maximum
OBJ_Relative_Velocity_Amp	maximum
OBJ_Relative_Velocity_x	minimum
OBJ_Relative_Velocity_y	minimum
OBJ_Relative_Velocity_z	minimum
OBJ_Separation_Overload_of_L_Amp	maximum
OBJ_Separation_Overload_of_L_x	minimum
OBJ_Separation_Overload_of_L_y	minimum
OBJ_Separation_Overload_of_L_z	minimum

A key step in the design of the experiment within ADAMS insight is the setting of the sampling parameters, where the variables set in the previous section are added to the experimental influences and a random sample is set.

A normality test on the sample set generated by ADAMS found that the random sample data set generated by the set variables followed a normal distribution.

Separation parameters meet the performance index calculation

After completing the experimental design, the simulation test is run. This simulation test is a total of 3000 rounds of cycle, time 4 hours and 47 minutes. After each simulation, the programme will automatically collect the simulation target parameters are specified as follows:

Relative separation speed between modules

The performance index of the relative separation velocity between the upper and lower modules is $\not<$0.4 m/s. According to the simulation model, it can be inferred that the main source of angular velocity is the spring group, disconnector and separating plug fixed between the upper and lower modules, and the thrust resistance generated between the two compartments at the stage of separation, as shown in the scatter diagram of angular velocity amplitude generated after randomly hitting the target 3,000 times, Table 5 is a overview of angular velocity, Figs. 6 and 7 describe the data distribution:

https://doi.org/10.1017/aer.2025.10063 Published online by Cambridge University Press

https://doi.org/10.1017/aer.2025.10063 Published online by Cambridge University Press

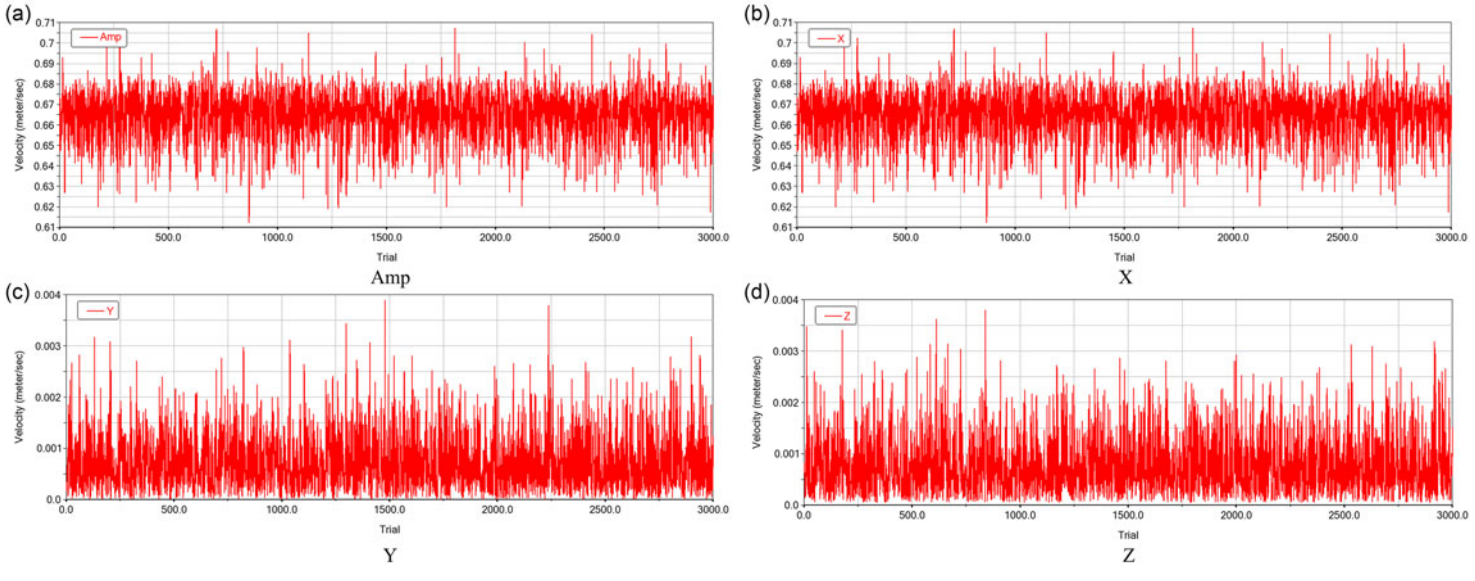


Figure 6. *Distribution of relative separation velocity data between upper and lower modules.*

Table 5. *Overview of angular velocity*

Parameter	Overload
Sample size	3000
Median	0.357
Average value	0.357
Standard deviation	0.022
Skewness	0.059
Kurtosis	−0.035
S-W Tests	0.999(0.411)
K-S Tests	0.011(0.855)

Table 6. *Overview of relative velocity*

Parameter	Overload
Sample size	3000
Median	0.667
Average value	0.665
Standard deviation	0.013
Skewness	−0.631
Kurtosis	0.632
S-W Tests	0.972(0.000)
K-S Tests	0.069(0.000)

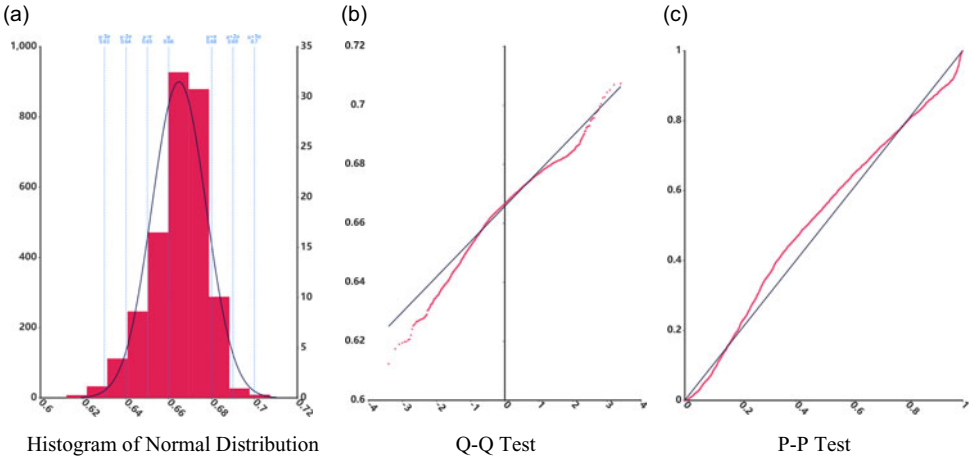


Figure 7. *Normality test for relative separation velocity between upper and lower modules.*

According to the results measured by the simulation target of the relative separation velocity between upper and lower modules, it can be seen that the relative separation velocity between upper and lower modules is mainly distributed in the x-direction, and the data show a spindle-shaped distribution, with less on both sides and more in the middle, mainly concentrated near 0.667 m/s.

The data are further tested and analysed for normality.

It can be seen that the relative separation speed data between upper and lower modules basically conforms to a normal distribution. The specific data are shown in the Table 6.

Random target shooting calculations show that the relative separation amplitude between the upper and lower modules is in the range of [0.612,0.707], and its performance specification is $\not<$0.4 m/s, so it satisfies the performance specification.

https://doi.org/10.1017/aer.2025.10063 Published online by Cambridge University Press

Angular acceleration of separation of the upper module

The upper module separation angular velocity performance index is required to be $\nearrow$1.2 deg/s. According to the simulation model, it can be inferred that the main source of its angular velocity is the y-direction tilting force brought by the asymmetric design of the spring, and the angular velocity dataset generated after 3,000 times of random target hitting is shown in Fig. 8.

According to the results of the separation angular velocity of the upper module, it can be seen that the separation angular velocity of the upper module is mainly distributed in the y-direction, and the data show a spindle-shaped distribution, with less on either side and more in the middle, mainly concentrated around 0.357 deg/s.

The data are further checked and analysed for normality in Fig. 9.

It can be seen that the separation angular velocity data of the upper module basically conforms to the normal distribution. The specific data are shown in the Table 5.

Random target shooting calculations show that the upper module separation angular velocity amplitude range is [0.282,0.43], while its performance specification is $\nearrow$1.2 deg/s, so it meets the performance specification. The overview of Overhold is shown in Table 7.

Overload of separation of lower module

The separation overload performance index of the lower modules is required to be $\nearrow$0.7 g, and according to the simulation model, it can be assumed that the overload mainly comes from the spring group, disconnector and separation plug fixed between the upper and lower modules, and the thrust resistance to the two compartments in the separation stage, as shown in Fig. 10. The separation overload data set of the lower modules generated after 3,000 times of random target hits.

According to the results of the lower module separation overload simulation target, it can be seen that the lower module separation overload is mainly distributed in the x-direction, and the data show a spindle-shaped distribution, with fewer on both sides and more in the middle, which is mainly concentrated around 5.228 m/s^2.

The data are further tested and analysed for normality in Fig. 11.

Random target calculations show that the lower module separation overload amplitude is in the range [4.51,5.997], while its performance specification is $\nearrow$0.7 g (6.86 m/s^2), so it meets the performance specification.

Collision analysis

In this paper, the safety and success of the separation process is assessed by measuring whether or not the contact force is generated between the main components of the upper and lower modules.

From the above Fig. 12 it can be concluded that the contact force between the upper and lower modules was always 0 during the simulation of the 3000 rounds. Therefore, it was judged that all simulated rounds were safely and successfully separated.

It can be seen in Fig. 13 that the on-orbit separation performance of the separation system fully meets the design requirements and its reliability reaches 100%.

Dynamic change of separation gap

The core of reliability assessment for separation based on the separation gap between upper and lower cabin modules lies in analysing whether the gap between modules during the separation process meets the requirements of collision-free and smooth separation, which necessitates the integration of multi-dimensional data to quantify the correlation between the gap and reliability.

5.0 Parameter importance analysis based on adaboost regression

The Adaboost regression algorithm gives a high weight to learners with a low error rate and a low weight to learners with a high error rate, combining the weak learners and the corresponding weights to generate strong learners. The difference between the regression and classification algorithms is that the error rate is calculated in a different way. Classification problems generally use a 0/1 loss function, while regression problems generally use a squared loss function or a linear loss function.

https://doi.org/10.1017/aer.2025.10063 Published online by Cambridge University Press

https://doi.org/10.1017/aer.2025.10063 Published online by Cambridge University Press

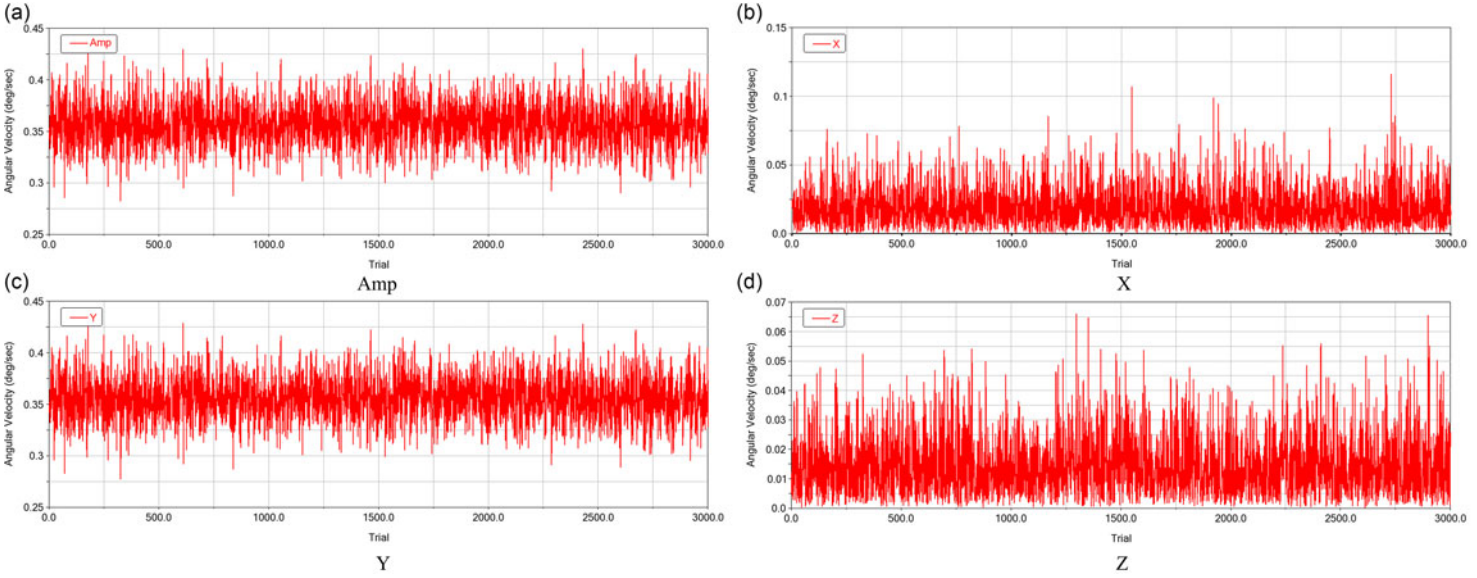


Figure 8. *Distribution of separation angular velocity data for the upper module.*

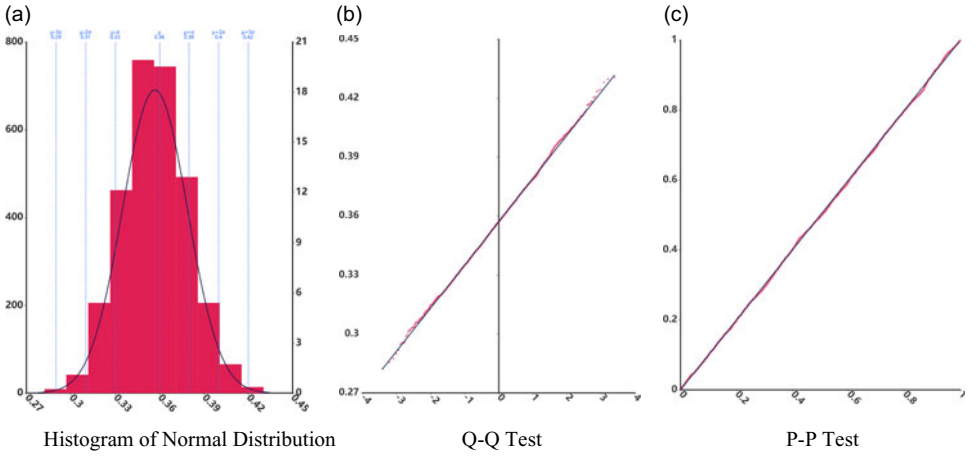


Figure 9. *Upper module separation angular velocity normality test.*

Table 7. *Overview of overload*

Parameter	Overload
Sample size	3000
Median	5.232
Average value	5.235
Standard deviation	0.079
Skewness	0.134
Kurtosis	−0.042
S-W Tests	0.999(0.012**)
K-S Tests	0.02(0.162)

The AdaBoost algorithm can be used not only for classification tasks but also for regression tasks. In this section, the parameter set of separation dynamics formed by ADAMS simulation is used to analyse the degree of influence of error inputs obeying normal distribution on the performance of the spacecraft separation system based on Adaboost regression.

Suppose there is a dataset that consists of m samples as follows:

$$D = \left\{ (x_1, y_1), (x_2, y_2), \ldots, (x_m, y_m) \right\} \tag{19}$$

Among them, $x_i \in \mathbf{R}^d$, means each sample data has d features, y_i is the target value. The specific steps of the AdaBoost regression algorithm are as follows in Fig. 14.

Take relative velocity as an example. The model parameters are set as Table 8.

The existing separation performance data is sliced and reorganised for training and testing through three steps: data slicing, data shuffling and cross-validation.

In the following Fig. 15, the prediction evaluation metrics of the cross-validation set, the training set and the test set are shown to measure the prediction effect of Adaboost through quantitative metrics. Among them, the evaluation metrics of the cross-validation set can continuously adjust the hyperparameters to get a reliable and stable model. Tables 9–11 shows the module assessment results of seperation parameter.

From the analysis results in Fig. 16, it can be seen that the maximum preload of the separation spring has a significant effect on the separation overload of the lower module and the relative separation speed of the two modules, which are 60.50% and 46.70%, respectively, followed by the mass of the lower module, which is 37.60% and 22.70%, respectively; the variables that have significant effects on the

https://doi.org/10.1017/aer.2025.10063 Published online by Cambridge University Press

https://doi.org/10.1017/aer.2025.10063 Published online by Cambridge University Press

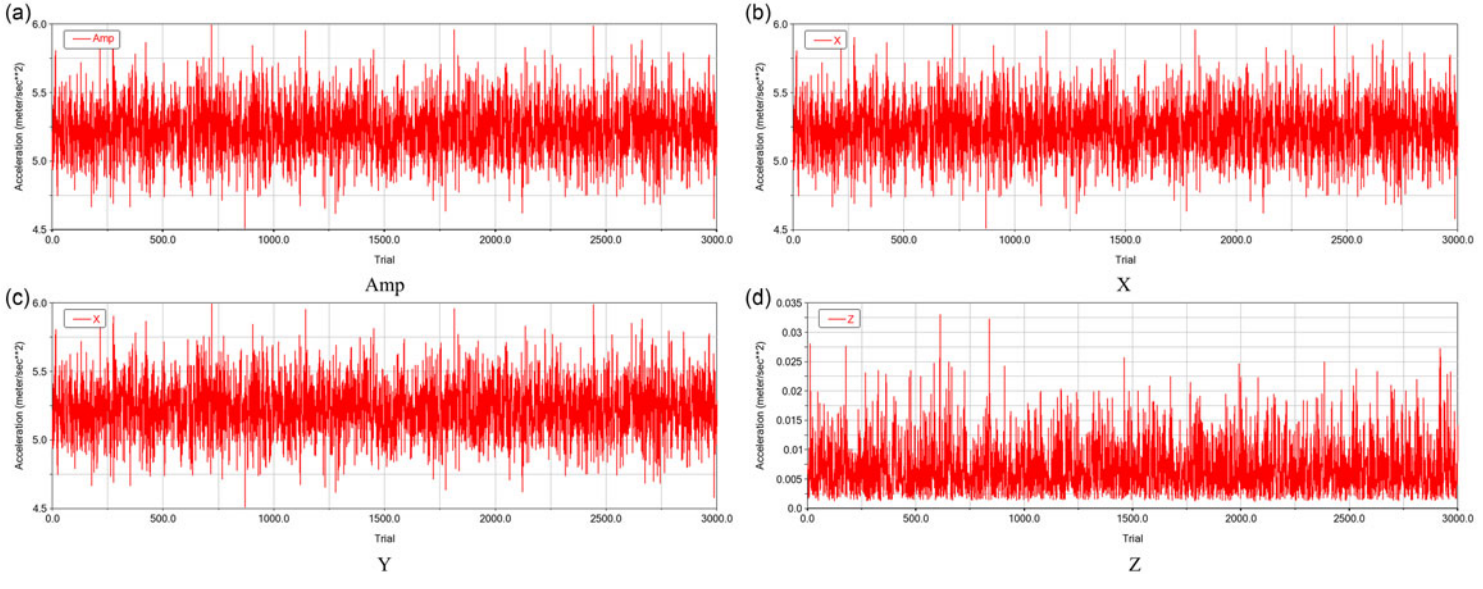


Figure 10. *Lower module separation overload data distribution.*

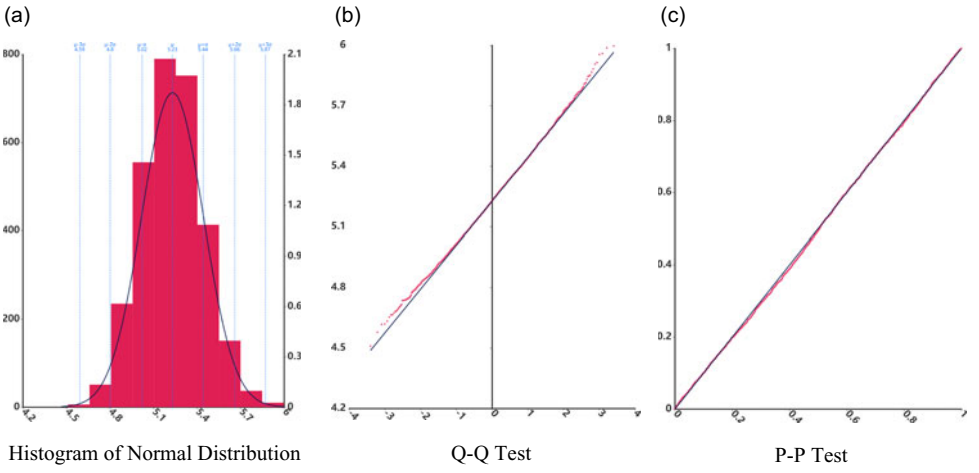


Figure 11. *Lower module separation overload normality test.*

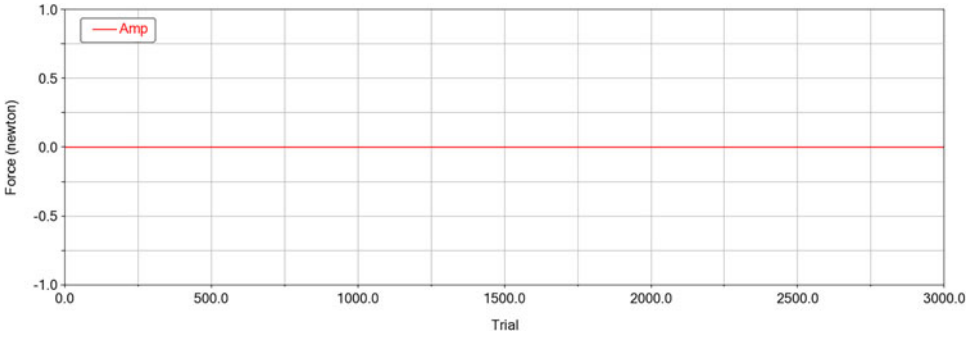


Figure 12. *Upper and lower modules collision detection.*

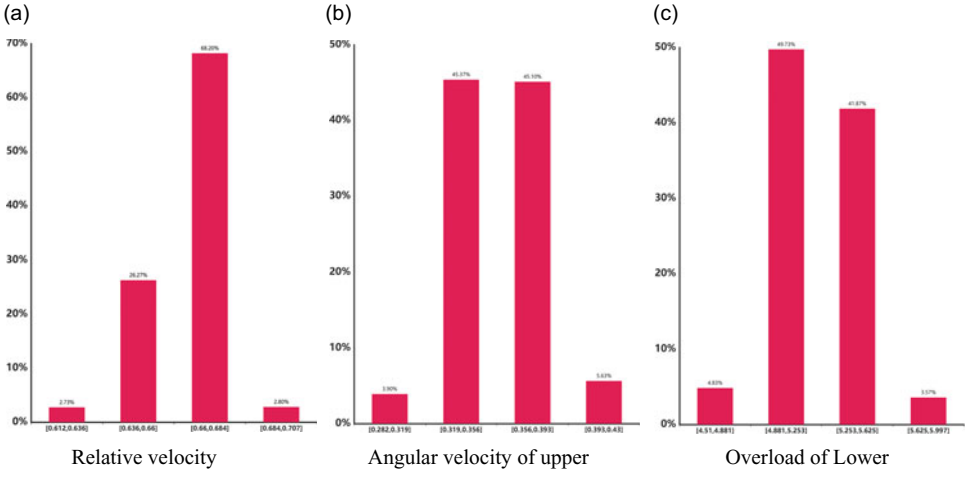


Figure 13. *Separation performance distribution.*

https://doi.org/10.1017/aer.2025.10063 Published online by Cambridge University Press

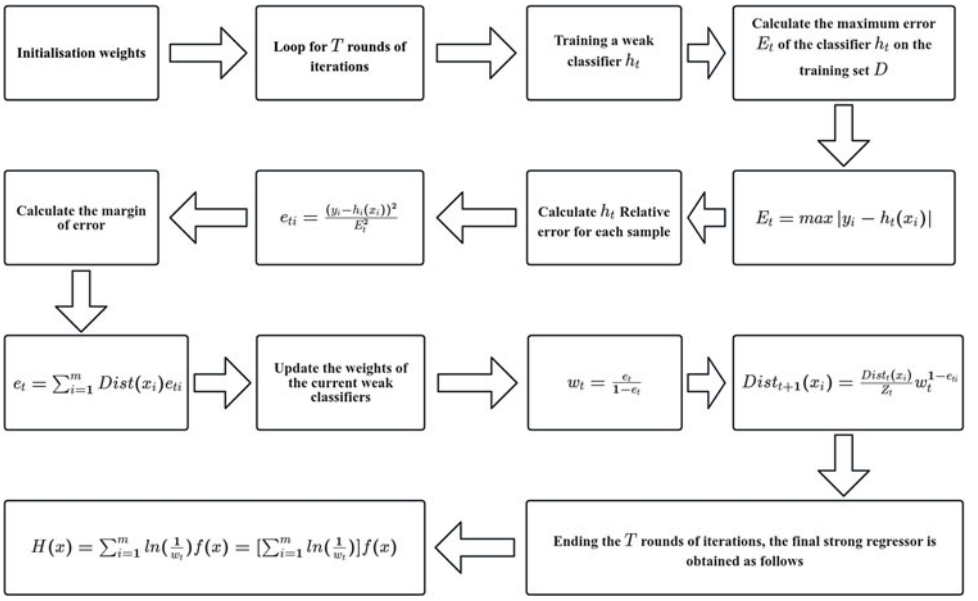


Figure 14. *Adaboost regression algorithm steps.*

Table 8. *Regression model parameterisation*

Parameter Name	Parameter Value
Training time	12.949 s
Data slice	0.7
Data shuffle	Yes
Cross-validation	50%
Number of base classifiers	100
Loss function	linear
Base classifier	Decision Tree Classifier
Learning rate	1

angular speed of the upper module separation are the Z-axis coordinates of the centre of mass of the upper module and the rotational moment of inertia of the upper module, which are 22.20% and 22.20%, respectively. 22.20% and 29.40%, respectively.

6.0 Conclusions

This paper analyses the reliability and design variable sensitivity of the spacecraft separation system by using Monte Carlo methods. The kinematics and dynamics of the separation system are investigated, the actual model and separation of the upper and lower modules are analysed using numerical analysis and simulation models, and the separation dynamics model of the upper and lower modules, which contains 23 groups of variables and 12 groups of targets, is built in the ADAMS multibody dynamics software. The study demonstrates that the relative separation velocity amplitude between the upper and lower modules is in the range of [0.612,0.707] m/s, the upper module separation angular velocity amplitude range is [0.282,0.43] deg/s, the lower module separation overload amplitude is in the range [4.51,5.997] m/s and all simulations show that the separation process is collision-free.

It can be concluded that the maximum preload of the separation spring, the mass of the lower module, the Z-axis coordinates of the centre of mass of the upper module and the moment of inertia of the

https://doi.org/10.1017/aer.2025.10063 Published online by Cambridge University Press

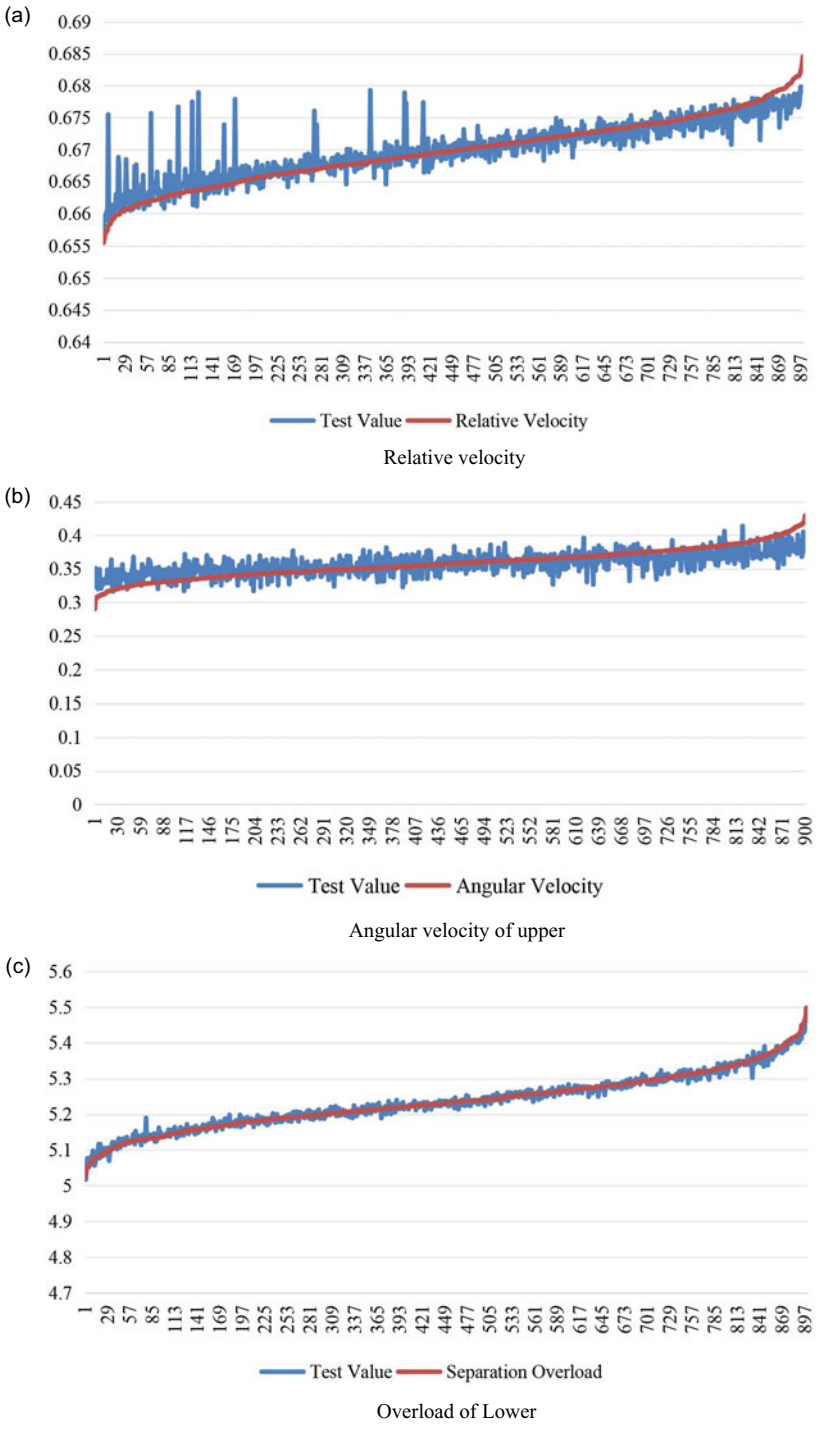


Figure 15. *Adaboost regression prediction.*

https://doi.org/10.1017/aer.2025.10063 Published online by Cambridge University Press

Table 9. *Module assessment results of relative velocity*

	MSE	RMSE	MAE	MAPE	R^2
Training set	0	0	0	0	1
Cross-validation set	0	0.002	0.002	0.236	0.8
Test set	0	0.002	0.001	0.223	0.819

Table 10. *Module assessment results of angular velocity*

	MSE	RMSE	MAE	MAPE	R^2
Training set	0	0	0	0.005	1
Cross-validation set	0	0.015	0.012	3.333	0.479
Test set	0	0.015	0.012	3.33	0.516

Table 11. *Module assessment results of separation overload*

	MSE	RMSE	MAE	MAPE	R^2
Training set	0	0	0	0	1
Cross-validation set	0	0.01	0.008	0.153	0.982
Test set	0	0.011	0.008	0.153	0.981

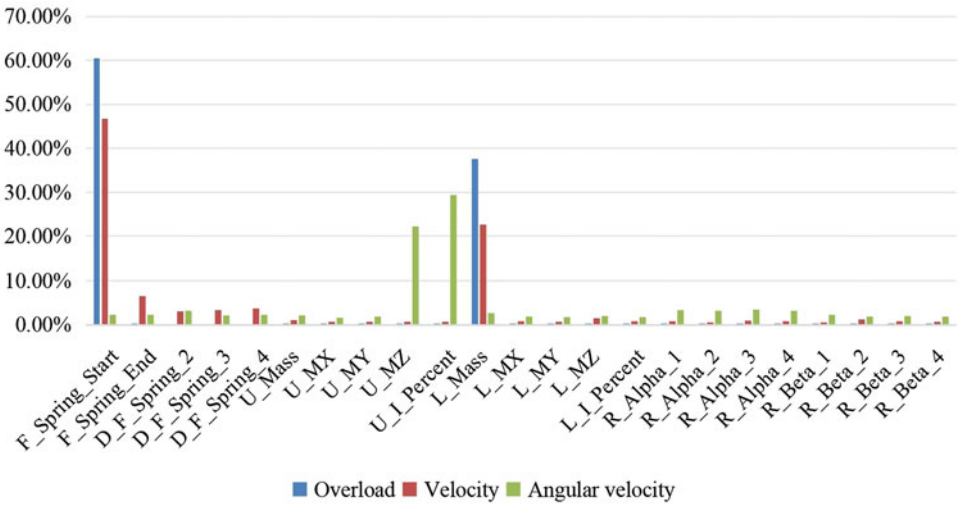


Figure 16. *Parameter sensitivity distribution.*

upper module have a great influence on the separation dynamics of the spacecraft, and the design and manufacture should focus on reducing their error ranges, so as to obtain a more accurate evaluation of the performance of the separation system.

7.0 On-orbit validation

In December 2024, the reusable spacecraft studied in this article, developed by the Shanghai Institute of Aerospace Systems Engineering (SIASE), was released on orbit for separation and successfully operated, and the actual measured values of the angular velocity of the spacecraft and the overload of the lower module during the separation process fell within the prediction intervals of the Monte Carlo stochastic target. They also met the design specifications for separation performance. During the actual

https://doi.org/10.1017/aer.2025.10063 Published online by Cambridge University Press

on-orbit separation mission, the assembled body has a trace initial angular velocity in the pitch, roll and yaw directions, which is input into the model built in this paper, and the output results still have stability and reliability.

Acknowledgments. This study was supported by a grant from the *Postgraduate Research & Practice Innovation Program of Jiangsu Province* (SJCX25_0161), 'Separation System of Heavy Launch Vehicle Interstage with Non-Fireworks Low Impact Belt Connection'. And Open *Project of National Key Laboratory of Aerospace Mechanism* (2025ASM-ZN10), 'Research on preload gradual release or stepwise release technology'.

References

[1] Wang, C., Nie, H. and Chen, J. The design and dynamic analysis of a lunar lander with semi-active control, *Acta Astronaut.*, 2019; **157**, pp 145–156.
[2] Hou, S., Li, D., Li, Q. and Tang, X. Force-transmission characteristics of a cable-driven mechanism with high initial velocity for spacecraft separation in ground tests, *J. Mech. Sci. Technol.*, 2023; **37**, (12), pp 6311–6324.
[3] Cui, D., Zhao, J., Yan, S., Guo, X. and Li, J. Analysis of parameter sensitivity on dynamics of satellite separation, *Acta Astronaut.*, 2015; **114**, pp 22–33.
[4] Yue, H., Yang, Y., Lu, Y., et al. Research progress of space non-pyrotechnic low-shock connection and separation technology (SNLT): A review, *Chin. J. Aeronaut.*, 2022; **35**, (11), pp 113–154.
[5] Hu, X., Chen, X., Zhao, Y. and Yao, W. Optimization design of satellite separation systems based on Multi-Island Genetic Algorithm, *Adv. Space Res.*, 2014; **53**, (5), pp 870–876.
[6] Rao, B.N., Jeyakumar, D., Biswas, K.K., Swaminathan, S. and Janardhana, E. Rigid body separation dynamics for space launch vehicles, *Aeronaut. J.*, 2016; **110**, (1107), pp 289–302.
[7] Saki, S., Bolandi, H. and Mousavi Mashhadi, SK-e-d. Optimal direct adaptive soft switching multi-model predictive control using the gap metric for spacecraft attitude control in a wide range of operating points, *Aerosp. Sci. Technol.*, 2018; **77**, pp 235–243.
[8] Li, W.-J., Cheng, D.-Y., Liu, X.-G., et al. On-orbit service (OOS) of spacecraft: A review of engineering developments, *Progr. Aerosp. Sci.*, 2019; **108**, pp 32–120.
[9] Ding, J., Zhao, H., Wang, J., Sun, Y. and Chen, Z. Numerical and experimental investigation on the shock mitigation of satellite-rocket separation, *Aerosp. Sci. Technol.*, 2020; **96**, p 105538.
[10] Fu, J., Liu, M., Cao, X. and Li, A. Robust neural-network-based quasi-sliding-mode control for spacecraft-attitude maneuvering with prescribed performance, *Aerosp. Sci. Technol.*, 2021; **112**, p 106667.
[11] Hou, S.H., Sun, H.N., Li, Q.Z. and Tang, X.Q. Design and experimental validation of a disturbing force application unit for simulating spacecraft separation, *Aerosp. Sci., Technol.*, 2021; **113**, p 106674.
[12] Lyu, B., Liu, C. and Yue, X. Hybrid nonfragile intermediate observer-based T-S fuzzy attitude control for flexible spacecraft with input saturation, *Aerosp. Sci. Technol.*, 2022; **128**, p 107753.
[13] Hu, Y., Wu, M., Zhao, K., Song, J. and He, B. ADRC-based compound control strategy for spacecraft multi-body separation, *Aerosp. Sci. Technol.*, 2023; **143**, p 108686.
[14] Luo, C., Sun, J., Wen, H. and Jin, D. Autonomous separation deployment dynamics of a space multi-rigid-body system with uncertain parameters, *Mech. Mach. Theory*, 2023; 180.
[15] Teng, L. and Jin, Z.-h. A composite optimization method for separation parameters of large-eccentricity pico-satellites, *Front. Inf. Technol. Electron. Eng.*, 2018; **19**, (5), pp 685–698.
[16] Merler, S., Caprile, B. and Furlanello, C. Parallelizing AdaBoost by weights dynamics, *Comput. Statist. Data Anal.*, 2007; **51**, (5), 2487–2498.
[17] Rokach, L. Taxonomy for characterizing ensemble methods in classification tasks: A review and annotated bibliography, *Comput. Statist. Data Anal.*, 2009; **53**, (12), pp 4046–4072.
[18] Tsao, C.A. and Chang, Y.-cI. A stochastic approximation view of boosting, *Comput. Statist. Data Anal.*, 2007; **52**, (1), pp 325–334.
[19] Aslanov, V., Kruglov, G. and Yudintsev, V. Newton–Euler equations of multibody systems with changing structures for space applications, *Acta Astronaut.*, 2011; **68**, (11–12), pp 2080–2087.

https://doi.org/10.1017/aer.2025.10063 Published online by Cambridge University Press

Appendix

Table 12. *Random sampling setup for variables obeying normal distribution*

Abbreviation	Name	Settings	Nominal Value	Dist Params
D F Spring_2	D F Spring_2	−25.25	0	8.33333
D F Spring_3	D F Spring_3	−25,25	0	8.33333
D F Spring_4	D F Spring_4	−25,25	0	8.33333
F_Spring_End	F_Spring_End	−30,30	533.5	10
F_Spring_Start	F_Spring_Start	−75,75	2177	25
L_I_Percent	L_I_Percent	−0.1,0.1	1	0.0333333
L_Mass	L_Mass	−40,40	1412.7	13.3333
L_MX	L_MX	−0.026,0.026	0.725	0.00866667
L_MY	L_MY	−0.01,0.01	−0.002	0.00333333
L_MZ	L_MZ	−0.011,0.011	−0.043	0.00366667
R_Alpha_1	R_Alpha_1	−0.0120131,0.	0	0.00400437
R_Alpha_2	R_Alpha_2	−0.0120131,0.	0	0.00400437
R_Alpha_3	R_Alpha_3	−0.0120131,0.	0	0.00400437
R_Alpha_4	R_Alpha_4	0.0120131,0.	0	0.00400437
R_Beta_1	R_Beta_1	−3.14,3.14	3.14	–
R_Beta_2	R_Beta_2	−3.14,3.14	3.14	–
R_Beta_3	R_Beta_3	−3.14,3.14	3.14	–
R_Beta_4	R_Beta_4	−3.14,3.14	3.14	–
U_I_Percent	U_I_Percent	−0.1,0.1	1	0.0333333
U_Mass	U_Mass	−15,15	3016.9	5
U_MX	U_MX	0.016,0.016	5.336	0.00533333
U_MY	U_MY	−0.01,0.01	−0.001	0.00333333
U_MZ	U_MZ	−0.011,0.011	0.037	0.00366667

Cite this article: Lai S., Wang T., Zhao Q., Wang C. and Chen J. (2025). Performance reliability and parameter sensitivity analysis of spacecraft separation system combining Monte Carlo and Adaboost regression methods. *The Aeronautical Journal*, **129**, 3665–3686. https://doi.org/10.1017/aer.2025.10063

https://doi.org/10.1017/aer.2025.10063 Published online by Cambridge University Press